polymer papers

Characterization of orientation of one-way and two-way drawn isotactic polypropylene films

I. Karacan, A. K. Taraiya, D. I. Bower and I. M. Ward*
IRC in Polymer Science and Technology, University of Leeds, Leeds LS2 9JT, UK
(Received 26 June 1992; revised 18 November 1992)

X-ray diffraction, Fourier Transform infra-red (*FT*i.r.) spectroscopic and refractive index measurements have been utilized to characterize the state of molecular orientation in one-way and two-way (biaxially) drawn isotactic polypropylene (iPP) films. It is shown that the use of all three techniques leads to much greater confidence in the orientation averages deduced than can be obtained by using any two of the techniques. Orientation parameters in terms of $\langle\cos^2\theta\rangle$ values in machine, transverse and normal directions have been evaluated and compared quantitatively for the different techniques. The results indicate that with one-way drawing the chain axes of both crystalline and amorphous regions orient towards the direction of drawing. The crystalline chains are more highly oriented than the amorphous chains and tend to orient towards the plane of the film, whereas the amorphous chains tend to be more uniaxially oriented towards the draw direction. In balanced, simultaneously two-way drawn films the crystalline chains are more highly oriented towards the plane of the film than the non-crystalline chains. For a sequentially, equibiaxially drawn iPP film, the orientations of the chain axes of both the crystalline and amorphous regions were found to be higher in the second draw (i.e. transverse) direction than in the first draw direction. The orientation of the crystalline chains was very close to the plane of the film, whereas the amorphous chains were almost uniaxially oriented with respect to the second draw direction. In all the films there is a strong tendency for the b-axes of the crystallites to align normal to the plane of the film.

(Keywords: isotactic polypropylene; orientation; *FT* i.r. spectroscopy; X-ray diffraction; one-way drawing; two-way drawing)

INTRODUCTION

The structure and properties of isotactic polypropylene (iPP) polymers have been the subject of many investigations[1–8], including X-ray diffraction[1,2], optical[3] analysis, infra-red[4,5] analysis, barrier properties[6,7] and mechanical modelling[8]. In the present investigation, one-way drawn, sequentially two-way drawn and simultaneously two-way drawn films of isotactic polypropylene have been studied with the aim of establishing as accurately as possible the states of orientation of the crystalline and amorphous chains, with the ultimate aim of gaining a better understanding of processing–structure–property relationships.

Molecular orientation measurements have been carried out using X-ray diffraction, *FT*i.r. spectroscopic and refractive index measurements. Each of the three techniques gives different information about the distribution of orientations and each suffers from uncertainties that are difficult to quantify. X-ray scattering can in principle give the complete distribution of orientations for the crystallites but suffers from difficulties in correcting for the background scattering due to amorphous material and other effects. Refractive index data can give only rather limited information about the distribution of orientations and even that information is more uncertain for polypropylene than for many other polymers because of uncertainty about the maximum birefringence of crystalline and amorphous material. Infra-red spectroscopy can give rather more information in principle than refractive index measurements, but there are difficulties in knowing whether individual absorption peaks provide information about crystalline or highly ordered chains only, or give some average over both. Using all three techniques helps both to resolve these problems and to provide more information than could be obtained using any one or two of them.

The function that describes the distribution of orientations of the structural units in a biaxially oriented polymer may be written in the form[9,10]

$$N(\theta,\phi,\psi)=\Sigma P_{lmn}Z_{lmn}(\cos\theta)e^{-im\phi}e^{-in\psi} \qquad (1)$$

where θ, ϕ and ψ are the Euler angles relating axes fixed within each unit to the symmetry axes fixed in the sample and $N(\theta,\phi,\psi)\sin\theta\,d\theta\,d\phi\,d\psi$ is the fraction of units whose axes lie in the generalized solid angle $\sin\theta\,d\theta\,d\phi\,d\psi$ at (θ,ϕ,ψ). The expression is in terms of generalized spherical harmonics with coefficients P_{lmn}. Infra-red spectroscopy can give information only about the coefficients P_{2mn} for m or $n=0$ or 2, i.e. P_{200}, P_{202}, P_{220} and P_{222}.

The coefficient P_{200} is the well known average over the second-order Legendre polynomial $\langle P_2(\cos\theta)\rangle=\frac{1}{2}(3\langle\cos^2\theta\rangle-1)$, where θ is the angle between the chain

* To whom correspondence should be addressed

0032-3861/93/132691-11

axis and a symmetry axis in the sample, usually chosen as the draw direction in a uniaxially or one-way drawn sample. The coefficient P_{220} is a measure of the departure from uniaxial symmetry of the chain axis distribution and is zero for true uniaxial symmetry around the chosen reference axis. The coefficient P_{202} is zero if there is no preferred orientation of the chains around their own axes and the coefficient P_{222} is zero if either the sample is uniaxial or there is no preferred orientation of the chains around their own axes.

Because it is not easy to understand the precise meaning of a particular set of numerical values of the P_{2mn}, they are converted into values of $\langle\cos^2\theta_{c,i}\rangle$, where $\theta_{c,i}$ is the angle between the chain axis and one of the symmetry axes of the sample (see ref. 9 for conversion equations). It is, however, useful to work with the P_{2mn} in the first instance as the mathematical development is simplified in this way.

EXPERIMENTAL DETAILS AND PRIMARY DATA ANALYSIS

Materials

In this work two grades of ICI polypropylene were used, a homopolymer grade PXC 34029 [MFI (230/2.16) = 7.4, called ICI PP in the tables] produced by supported catalyst gas-phase technology and a copolymer grade GPE102 [MFI (230/2.16) = 0.4] containing 10% of an ethylene/propylene copolymer. The copolymer feedstock was obtained in the form of commercially available sheets 1.5 mm thick. Homopolymer sheets were made by pressure moulding from polymer chips at 210°C followed by quenching in water at room temperature to produce sheets of thickness in the range 0.4–1.4 mm.

The homopolymer samples were drawn in a hot-air oven on an Instron tensile-testing machine with gauge length 20 mm × 100 mm wide at a crosshead speed of 20 mm min^{-1} and a draw temperature of 155°C. The simultaneously biaxially drawn samples of homopolymer were drawn at 155°C using the Long stretcher located at ICI Films, Welwyn Garden City. This machine operates on smaller sheets (~100 mm × 100 mm dimensions). Samples E, F and G of the present study are three of the same PXC 34029 polypropylene samples used in ref. 11.

The copolymer samples were drawn at 155°C from isotropic sheets 230 mm × 230 mm × 1.5 mm at a crosshead speed of 600 mm min^{-1} on a Bruckner two-way stretching machine that allows simultaneous or sequential drawing along two perpendicular directions in a hot-air oven. Sample details are given in *Table 1*.

Density measurements and crystallinity

Density measurements were carried out with a graded density column obtained from mixtures of propan-2-ol and diethylene glycol (digol) to give a density range from 0.860 to 0.925 g cm^{-3}. Fractional volume crystallinity was evaluated from the densities using a two-phase model and assuming the crystalline and amorphous densities to be 0.936 and 0.853 g cm^{-3}, respectively[12]. The densities and the fractional crystallinities of the samples are presented in *Table 1*.

Refractive index measurements

Refractive index measurements were carried out with a Bellingham and Stanley Abbe refractometer using

Table 1 Sample details

Sample	Polymer grade	Draw ratios	Refractive indices			Density (g cm^{-3})	v_c[a]
			n_M	n_T	n_N		
A	ICI PP	8.5 × 0.9	1.5289	1.4994	1.5007	0.9132	0.7253
						∓0.0002	∓0.0023
B	ICI PP	9.5 × 0.9	1.5306	1.4994	1.5007	0.9130	0.7225
						∓0.0002	∓0.0022
C	ICI PP	12.0 × 0.8	1.5323	1.4985	1.4994	0.9121	0.7115
						∓0.0002	∓0.0022
D	ICI PP	14.0 × 0.8	1.5332	1.4994	1.5003	0.9118	0.7087
						∓0.0002	∓0.0023
E	ICI PP	4.5 × 4.5	1.5143	1.5105	1.5019	0.9120	0.7108
						∓0.0002	∓0.0023
F	ICI PP	6.0 × 6.1	1.5143	1.5118	1.5019	0.9115	0.7048
						∓0.0002	∓0.0023
G	ICI PP	7.5 × 7.5	1.5128	1.5102	1.4991	0.9101	0.6880
						∓0.0002	∓0.0022
H	GPE 102	7.5 × 1.0	1.5220	1.4931	1.4930	0.9066	0.6456
						∓0.0002	∓0.0023
I	GPE 102	7.5 × 7.5	1.5082	1.5143	1.5003	0.9005	0.5723
						∓0.0002	∓0.0023
J	GPE 102	7.5 × 7.8	1.5073	1.5074	1.4949	0.8985	0.5482
			∓0.0009	∓0.0009	∓0.0009	∓0.0006	∓0.0073

[a] Fractional crystallinity $= v_c = \dfrac{\rho-\rho_a}{\rho_c-\rho_a} = \dfrac{\rho-0.853}{0.936-0.853}$

α-bromonaphthalene as the optical contact liquid. The measurements were carried out using a sodium lamp source in a temperature-controlled room at 20 ± 1°C, and the results are shown in *Table 1*.

X-ray diffraction measurements

In order to describe the orientations of the crystallographic axes of crystallites in a polymeric material a three-dimensional coordinate system is introduced, as shown in *Figure 1*. Sample reference coordinate axes have been defined along the machine direction (M), transverse direction (T) and normal direction (N). For one-way drawn samples the machine direction is the draw direction and for sequentially drawn samples it is the first draw direction. The orientation of a unit vector normal to a given crystallographic plane can then be described by two angles α and β, where α is the angle between ON and the normal to the reflecting plane and β is the angle between the projection of that normal on the OMT plane and the OT direction.

$I(\alpha, \beta)$ is the intensity representing the relative amount of material having (*hkl*) plane normals in the direction α, β. Then

$$\langle \cos^2 \theta_{hkl,N} \rangle = \frac{\int_0^{2\pi} \int_0^{\pi/2} I(\alpha, \beta) \cos^2 \alpha \sin \alpha \, d\alpha \, d\beta}{\int_0^{2\pi} \int_0^{\pi/2} I(\alpha, \beta) \sin \alpha \, d\alpha \, d\beta} \quad (2)$$

$$\langle \cos^2 \theta_{hkl,T} \rangle = \frac{\int_0^{2\pi} \int_0^{\pi/2} I(\alpha, \beta) \sin^3 \alpha \cos^2 \beta \, d\alpha \, d\beta}{\int_0^{2\pi} \int_0^{\pi/2} I(\alpha, \beta) \sin \alpha \, d\alpha \, d\beta} \quad (3)$$

$$\langle \cos^2 \theta_{hkl,M} \rangle = \frac{\int_0^{2\pi} \int_0^{\pi/2} I(\alpha, \beta) \sin^3 \alpha \sin^2 \beta \, d\alpha \, d\beta}{\int_0^{2\pi} \int_0^{\pi/2} I(\alpha, \beta) \sin \alpha \, d\alpha \, d\beta} \quad (4)$$

In the absence of strong meridional reflections it is usually necessary to determine the crystalline orientation factor $\langle \cos^2 \theta_{c,i} \rangle$ indirectly from equatorial reflections. For iPP at least two equatorial reflections are necessary because of its monoclinic unit cell – for this study the (110) and (040) reflections were used. The calculations were carried out using Wilchinsky's method[13].

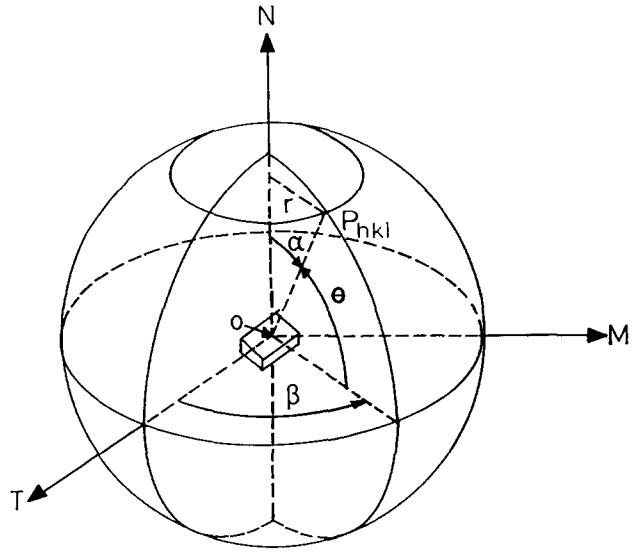

Figure 1 Position of pole *P* located by spherical coordinates α and β

Pole figure analysis and the determination of orientation functions of certain semicrystalline polymers are well documented in the literature[14,15]. In this study, the X-ray diffraction measurements were carried out using a computer-controlled Huber texture goniometer employing CuKα radiation.

The samples were prepared by parallel stacking of layers of drawn films to form a pad approximately 0.5 mm thick and 30 mm × 20 mm. Care was taken to match the draw directions by matching the grids on the drawn films. A poly(vinyl alcohol) (PVA) glue was used to prepare the stacks since it provided a strong bond yet gave little background scatter and no discrete X-ray diffraction peaks.

Each sample was scanned to measure the intensity as a function of α and β in both transmission and reflection modes, since neither mode can cover the whole range of α from 0 to 90°. The position of the detector was set at the 2θ angle corresponding to a selected (*hk*0) reflection, while the sample was tilted and rotated about its own axis to record the intensities of the diffracting planes in space. The intensities were recorded with circular scans, i.e. β-scans, at 10° intervals over the angular range $0° \leqslant \alpha \leqslant 90°$ and at 2° intervals over the angular range $0° \leqslant \beta \leqslant 360°$. Circular scans were performed by the reflection technique for $\alpha = 0$ to 50° and in transmission for $\alpha = 50$ to 90°.

The intensity data were corrected for background, defocusing and absorption effects. Background scatter was measured as a function of α and β at a 2θ position off the peak in reflection and transmission geometry. Defocusing and absorption corrections in reflection geometry were carried out using a random sample of the same thickness[14]. Absorption corrections in transmission geometry were carried out according to a procedure developed by Decker *et al.*[16].

After applying the corrections, the intensities obtained from the transmission and reflection measurements were scaled to the same level.

The values of $\langle \cos^2 \theta_{i,j} \rangle$ (where i = a, b or c and j = M, T or N) determined from the X-ray diffraction analysis are presented in *Table 2*.

Infra-red measurements

Experimental details. A Nicolet 740 Fourier Transform infra-red spectrometer equipped with a wire-grid polarizer positioned adjacent to the sample was employed for infra-red dichroic measurements. The beam passed first through the polarizer and then through the sample before reaching the detector. The polarizer remained in a fixed orientation throughout and the samples were rotated in order to obtain different polarized spectra.

In all cases 100 interferograms of a sample were averaged and transformed with the Happ–Genzel apodization function. Each sample spectrum was ratioed against a corresponding number of background scans using the same polarizer setting and instrument settings. The spectrometer was purged to minimize problems caused by water and carbon dioxide in the air. All the spectra were collected at a resolution of 1 cm^{-1}.

In order to measure the peak absorbances for radiation polarized in the plane of the film, i.e. in the machine or transverse direction, 'normal film' experiments

Table 2 Values of $\langle \cos^2 \theta_{i,j} \rangle$ obtained from X-ray diffraction

Sample		(T)	(N)	(M)
A (8.5 × 0.90)	(a)	0.56	0.41	0.03
(ICI PP)	(b)	0.40	0.58	0.02
	(c)	0.04	0.01	0.95
D (14.0 × 0.77)	(a)	0.61∓0.02	0.39∓0.01	0.01∓0.01
(ICI PP)	(b)	0.39∓0.01	0.59∓0.01	0.01∓0.01
	(c)	0.00∓0.02	0.02∓0.02	0.98∓0.01
E[a] (4.5 × 4.5)	(a)	0.33	0.35	0.32
(ICI PP)	(b)	0.21	0.59	0.20
	(c)	0.46	0.06	0.48
F[a] (6.0 × 6.1)	(a)	0.37	0.28	0.35
(ICI PP)	(b)	0.16	0.68	0.16
	(c)	0.47	0.04	0.49
G[a] (7.5 × 7.5)	(a)	0.37	0.26	0.37
(ICI PP)	(b)	0.16	0.70	0.14
	(c)	0.47	0.04	0.49
H (7.5 × 1.0)	(a)	0.51	0.42	0.07
(GPE 102)	(b)	0.40	0.56	0.04
	(c)	0.09	0.02	0.89
I[b] (7.5 × 7.5)	(a)	0.28	0.28	0.44
(GPE 102)	(b)	0.11	0.73	0.16
	(c)	0.61	−0.01	0.40
J[a] (7.5 × 7.8)	(a)	0.34	0.32	0.34
(GPE 102)	(b)	0.19	0.63	0.18
	(c)	0.47	0.05	0.48

[a] Simultaneously two-way drawn
[b] Sequentially two-way drawn

were performed with the plane of the film perpendicular to the beam. The film was sandwiched between potassium bromide plates. From these measurements, the peak absorbances A_M and A_T for radiation polarized parallel to the machine and transverse directions, respectively, were obtained for each absorption. 'Tilted film' experiments were carried out with the plane of the film tilted at 45° with respect to the beam in order to measure peak absorbances for radiation with a component of polarization in the normal direction, i.e. perpendicular to the plane of the film. For this purpose, the film was sandwiched between 45° prisms of potassium bromide. From these experiments, peak absorbances A_{TN} were obtained for polarization in the plane containing the transverse and normal directions and peak absorbances A_{MN} were obtained for polarization in the plane containing the machine and normal directions. In all cases, layers of nujol (liquid paraffin oil) were used to improve optical contact. The 750–1080 cm^{-1} 'clear region' of the nujol spectrum was employed in the analysis.

All the infra-red data were transferred to an Amdahl mainframe computer for data analysis, including curve fitting. The directly measured absorbance values from highly oriented samples were found to contain errors due to the fact that the polarizer transmits a small fraction of radiation polarized perpendicularly to its principal transmission direction. These errors were corrected according to a procedure developed by Green and Bower[17]. These corrections were found to be insignificant for the biaxially oriented samples, for which the true absorbance values rarely exceeded 1. The corrections for polarizer imperfection are a function of wavenumber, the thickness of the sample and the degree of orientation of the sample. For the 841 cm^{-1} peak of sample D, an uncorrected absorbance of 1.73 for the polarization in the direction of highest absorbance was recorded and a correction of almost 15% of the measured absorbance was necessary, corresponding to a change in $\langle \cos^2 \theta_{c,M} \rangle$ from 0.98 to 0.99.

Curve fitting of spectra. The infra-red spectrum of iPP in the 750–1080 cm^{-1} region has at least seven well defined absorption peaks, as shown in *Figure 2*. Of these peaks, those at 841, 973 and 998 cm^{-1} can be described as being very strong in intensity and showing parallel polarization characteristics, whereas the peaks at 809, 900 and 940 cm^{-1} can be described as being medium in intensity and showing perpendicular polarization characteristics. There is also a doublet with peaks at 1036 and 1045 cm^{-1}, both components of which are medium in intensity and show parallel polarization characteristics. During the curve-fitting procedures described below it was found necessary to resolve the peak at 973 cm^{-1} into two peaks, one at 972 cm^{-1} and another at 974 cm^{-1}, in order to improve the fitting (*Figure 3*). In addition to the major peaks, nine minor peaks were required at 796, 828, 834, 858, 923, 950, 962, 1004 and 1015 cm^{-1} to improve the fits in the tails of the major peaks, but they are not considered further.

All the spectra obtained from the normal film and tilted film experiments were fitted with Lorentzian peaks together with a linear background. Initially, the two

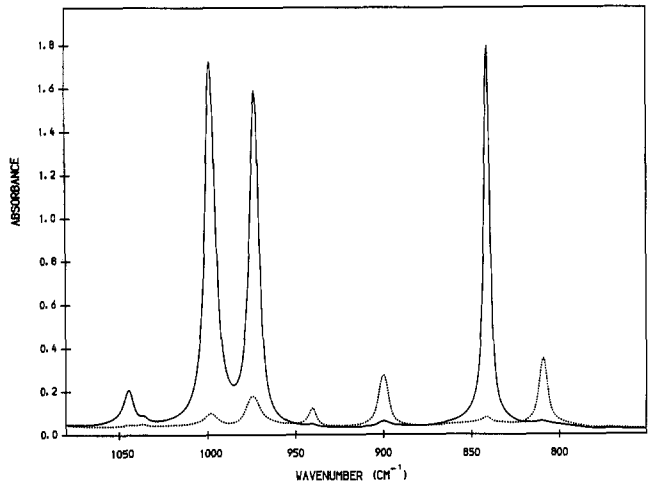

Figure 2 'Normal film' spectra of one-way drawn sample D: (——) polarization vector parallel to draw direction; (....) polarization vector perpendicular to draw direction

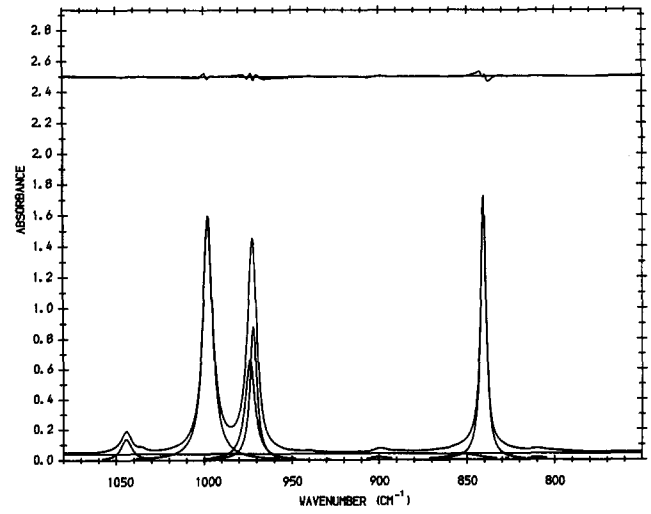

Figure 3 An example of curve fitting. The polarization direction is parallel to the draw direction. The lower curves are the fitted Lorentzian peaks, the middle curve is the observed curve and the upper curve is the difference between the fitted spectrum and the observed spectrum on the same scale

normal film spectra were fitted independently, allowing the peak positions and widths (full width at half peak height) to vary freely. In the final stages of the curve-fitting procedures, the peak positions and widths of the parallel peaks were fixed when fitting the perpendicular polarization spectrum while allowing the peak heights to vary freely. Conversely, the positions and widths of the perpendicular peaks were fixed when fitting the parallel polarization spectrum while allowing the peak heights to vary.

Finally, the tilted film spectra were fitted by fixing the positions and widths of all the peaks at the average values found from the fits of the normal film spectra and only allowing the peak heights to vary freely.

Evaluation of orientation averages. In general, if we know the transition moment angles within the structural unit and can measure the peak absorbances in the machine, transverse and normal directions, the orientation averages of the structural units with respect to the sample axes can be calculated[9,18].

In the present study, the procedure used by Jarvis *et al.*[9] was used for analysing the infra-red data. In this analysis the values of the imaginary parts k_i of the three complex refractive indices at each absorption peak are first calculated, where $i = M$, T or N, and the orientation parameters were then evaluated from the k_i. The steps in the calculation are as follows.

(i) The values of k_T and k_M were calculated from the experimentally measured peak absorbances A_T and A_M using the equation

$$k_i = A_i/(4\pi t\tilde{\nu}\log_{10} e) \tag{5}$$

where $i = T$ or M.

(ii) The values of k_N were calculated from the measured absorbances A_{TN} and A_{MN} and the equation

$$A_{jN}/\log_{10} e = 4\pi t\tilde{\nu}\left(\frac{n_j}{n_N}\right)\frac{n_N^2\kappa_j + n_0^2\sin^2\theta(\kappa_N - \kappa_j)}{\sqrt{n_N^2 - n_0^2\sin^2\theta}} \tag{6}$$

where $j = T$ or M, $k_i = n_i\kappa_i$ for $i = N$, M or T and $\theta = 45°$.

The optical refractive indices were used in this equation as an approximation to the infra-red refractive indices.

(iii) The values of k_N, k_M and k_T were used to calculate ϕ_N, ϕ_M and ϕ_T using the equation

$$\phi_i = 6n_ik_i/(n_i^2 + 2)^2 \tag{7}$$

where $i = N$, M or T.

In the calculation of ϕ_N, the mean value of k_N as determined from the peak absorbances A_{TN} and A_{MN} was used.

(iv) The orientation averages were obtained using the equations (cf. equations (23a, b) of ref. 9)

$$\frac{2\phi_M - \phi_T - \phi_N}{\phi_M + \phi_T + \phi_N} = 2p_{200}(\theta_m)P_{200} + 4p_{200}(\theta_m)P_{202} - 4P_{202} \tag{8}$$

and

$$\frac{\phi_T - \phi_N}{\phi_M + \phi_T + \phi_N} = 4p_{200}(\theta_m)P_{220} + \tfrac{4}{3}p_{200}(\theta_m)P_{222} - \tfrac{4}{3}P_{222} \tag{9}$$

The transition moment angles θ_m for the parallel peaks were assumed in the first analysis to be 0°, and for these peaks equations (8) and (9) reduce to

$$\frac{2\phi_M - \phi_T - \phi_N}{\phi_M + \phi_T + \phi_N} = 2P_{200} \qquad \text{for } \theta_m = 0° \tag{10}$$

and

$$\frac{\phi_T - \phi_N}{\phi_M + \phi_T + \phi_N} = 4P_{220} \qquad \text{for } \theta_m = 0° \tag{11}$$

For perpendicular peaks the transition moment angles were assumed in the first analysis to be 90° and for these peaks equations (8) and (9) reduce to

$$\frac{2\phi_M - \phi_T - \phi_N}{\phi_M + \phi_T + \phi_N} = -(P_{200} + 6P_{202}) \qquad \text{for } \theta_m = 90° \tag{12}$$

and

$$\frac{\phi_T - \phi_N}{\phi_M + \phi_T + \phi_N} = -2(P_{220} + P_{222}) \qquad \text{for } \theta_m = 90° \tag{13}$$

Although the parallel peak at 973 cm^{-1} was resolved into two components, it was at first assumed that both of these components were due to the same vibrational mode and the values of ϕ_i for the two components were averaged, weighting them in proportion to their widths. These average values of ϕ_i were then used in the calculations of P_{200} and P_{220}. The corresponding values of $\langle\cos^2\theta_{c,i}\rangle$ are shown in *Table 3* for the 841 and 973 cm^{-1} peaks.

The calculations of the P_{202} and P_{222} values for the perpendicular peaks were carried out by using the values of P_{200} and P_{220} from measurements on the peak at 841 cm^{-1} in equations (12) and (13), respectively.

FURTHER ANALYSIS AND DISCUSSION OF RESULTS

Amorphous orientation averages

The amorphous orientation averages were evaluated by combining the X-ray diffraction parameters and the optical refractive index measurements. It was assumed that the semicrystalline polymer was composed only of crystalline and amorphous phases, to each of which can be attributed specific anisotropic, intrinsic properties.

Since the two phases are additive we have the following equations

$$n_M - n_T = v_c\Delta_c^\circ(\langle\cos^2\theta_M\rangle - \langle\cos^2\theta_T\rangle)_c + (1 - v_c)(\langle\cos^2\theta_M\rangle - \langle\cos^2\theta_T\rangle)_a \tag{14}$$

$$n_M - n_N = v_c\Delta_c^\circ(\langle\cos^2\theta_M\rangle - \langle\cos^2\theta_N\rangle)_c + (1 - v_c)(\langle\cos^2\theta_M\rangle - \langle\cos^2\theta_N\rangle)_a \tag{15}$$

$$n_T - n_N = v_c\Delta_c^\circ(\langle\cos^2\theta_T\rangle - \langle\cos^2\theta_N\rangle)_c + (1 - v_c)(\langle\cos^2\theta_T\rangle - \langle\cos^2\theta_N\rangle)_a \tag{16}$$

where the subscripts c and a represent the crystalline and amorphous phases, respectively, v_c is the fractional volume crystallinity and Δ_c° and Δ_a° are the corresponding intrinsic birefringences of the crystalline and amorphous phases, respectively. These equations are derived on the assumption that the birefringences are small compared with the refractive indices and that the structural units

Table 3 Values of $\langle\cos^2\theta\rangle$ for parallel polarization i.r. peaks

Sample	Draw ratio	Peak (cm^{-1})	$\langle\cos^2\theta_{c,M}\rangle$	$\langle\cos^2\theta_{c,T}\rangle$	$\langle\cos^2\theta_{c,N}\rangle$
A	8.5 × 0.90	841	0.941	0.049	0.010
(ICI PP)		973	0.807	0.120	0.073
B	9.5 × 0.86	841	0.970	0.023	0.007
(ICI PP)		973	0.803	0.108	0.089
C	12.0 × 0.75	841	0.990	0.007	0.003
(ICI PP)		973	0.838	0.066	0.096
D	14.0 × 0.77	841	0.990∓0.002	0.007∓0.003	0.003∓0.002
(ICI PP)		973	0.843∓0.003	0.104∓0.003	0.053∓0.002
H	7.5 × 1.0	841	0.866	0.099	0.035
(GPE 102)		973	0.764	0.164	0.072
E[a]	4.5 × 4.5	841	0.466	0.407	0.127
(ICI PP)		973	0.437	0.394	0.169
F[a]	6.0 × 6.1	841	0.494∓0.002	0.452∓0.004	0.054∓0.003
(ICI PP)		973	0.461∓0.002	0.432∓0.004	0.107∓0.004
G[a]	7.5 × 7.5	841	0.482	0.477	0.041
(ICI PP)		973	0.459	0.454	0.087
I[b]	7.5 × 7.5	841	0.406	0.570	0.024
(GPE 102)		973	0.388	0.511	0.101
J[a]	7.5 × 7.8	841	0.502	0.489	0.009
(GPE 102)		973	0.487	0.479	0.034

[a] Simultaneously two-way drawn
[b] Sequentially two-way drawn

have transverse isotropy, both of which are true for polypropylene.

On rearrangement of the above equations we have

$$2n_M - n_T - n_N = v_c\Delta_c^\circ(3\langle\cos^2\theta_M\rangle - 1)_c + (1-v_c)\Delta_a^\circ(3\langle\cos^2\theta_M\rangle - 1)_a \quad (17)$$

$$2n_T - n_M - n_N = v_c\Delta_c^\circ(3\langle\cos^2\theta_T\rangle - 1)_c + (1-v_c)\Delta_a^\circ(3\langle\cos^2\theta_T\rangle - 1)_a \quad (18)$$

$$2n_N - n_M - n_T = v_c\Delta_c^\circ(3\langle\cos^2\theta_N\rangle - 1)_c + (1-v_c)\Delta_a^\circ(3\langle\cos^2\theta_N\rangle - 1)_a \quad (19)$$

which finally lead to the following equations

$$\langle\cos^2\theta_M\rangle_a = \tfrac{1}{3} + \frac{(2n_M - n_T - n_N) - v_c\Delta_c^\circ(3\langle\cos^2\theta_M\rangle - 1)_c}{3(1-v_c)\Delta_a^\circ} \quad (20)$$

$$\langle\cos^2\theta_T\rangle_a = \tfrac{1}{3} + \frac{(2n_T - n_M - n_N) - v_c\Delta_c^\circ(3\langle\cos^2\theta_T\rangle - 1)_c}{3(1-v_c)\Delta_a^\circ} \quad (21)$$

$$\langle\cos^2\theta_N\rangle_a = \tfrac{1}{3} + \frac{(2n_N - n_M - n_T) - v_c\Delta_c^\circ(3\langle\cos^2\theta_N\rangle - 1)_c}{3(1-v_c)\Delta_a^\circ} \quad (22)$$

The values of Δ_c° and Δ_a° for polypropylene have been given by Samuels[3] as 0.0291 and 0.060, respectively, whereas Masuko *et al.*[19] give 0.0416 and 0.0379. Hence the relative proportions of the crystalline and amorphous components in the equations will depend on which values are utilized. In the absence of any obvious reason to select either pair of intrinsic birefringence values, both sets of amorphous orientation values are presented for comparison in *Table 4*, where they are compared with the values obtained by the X-ray and infra-red techniques.

Infra-red results – parallel modes

841 cm^{-1}. This peak is the narrowest peak in the spectral region studied (3.7 cm^{-1}). It has been assigned to long, regular helical chains[20] most of which are likely to be present in the crystalline regions or similarly oriented to the chains in such regions. *Figure 4* shows a plot of P_{200} determined from the data for this peak using equation (10) against the values of P_{200} determined from X-ray diffraction. The agreement between the two sets of values is excellent. *Figure 5* shows a similar plot for the values of P_{220} determined using equation (11) against those determined from X-ray diffraction. Although the scatter is greater, there is overall agreement between the two sets of data. The conclusion is that this peak may be used for determining chain axis orientation for crystalline (or at least highly ordered) material where X-ray data are not available, as for samples B and C.

998 cm^{-1}. This peak has a width somewhat greater than that of the 841 cm^{-1} peak (6.3 cm^{-1}). It has usually also been assigned to crystalline or highly ordered material[21]. *Figure 6* suggests, however, that the P_{200} values obtained from equation (10) are always slightly lower than those obtained from the 841 cm^{-1} peaks, but tend to approach them as P_{200} tends to unity. This result is consistent with the assumption that this peak has its absorption dipole parallel to the chain axis for highly ordered material but is slightly sensitive to less highly ordered material, which is probably converted to more ordered material as P_{200} approaches unity. This is consistent with the finding that the 998 cm^{-1} peak remains even when the regular sequence length is reduced below 10 units[20]. The P_{220} values for the 841 and

Table 4 Values of $\langle \cos^2 \theta \rangle$ for the c-axis relative to the machine (M), transverse (T) and sheet normal (N) directions

Sample	Draw ratio		Characterization technique: X-ray diffraction	Characterization technique: *FT*i.r. (841 cm^{-1})	Amorphous[d]
A	8.5 × 0.90	(M)	0.950	0.941	0.711 (0.394)
(ICI PP)		(T)	0.040	0.049	0.086 (0.197)
		(N)	0.010	0.010	0.203 (0.409)
B	9.5 × 0.86	(M)		0.970	
(ICI PP)		(T)		0.023	
		(N)		0.007	
C	12.0 × 0.75	(M)		0.990	
(ICI PP)		(T)		0.007	
		(N)		0.003	
D	14.0 × 0.77	(M)	0.980	0.990	0.842 (0.620)
(ICI PP)		(T)	0.000	0.007	0.065 (0.176)
		(N)	0.020	0.003	0.093 (0.204)
E[a]	4.5 × 4.5	(M)	0.480	0.466	0.470 (0.430)
(ICI PP)		(T)	0.460	0.407	0.275 (0.138)
		(N)	0.060	0.127	0.256 (0.432)
F[a]	6.0 × 6.1	(M)	0.490	0.494	0.432 (0.367)
(ICI PP)		(T)	0.470	0.452	0.314 (0.196)
		(N)	0.040	0.054	0.253 (0.438)
G[a]	7.5 × 7.5	(M)	0.486	0.482	0.460 (0.423)
(ICI PP)		(T)	0.468	0.477	0.340 (0.247)
		(N)	0.046	0.041	0.200 (0.330)
H[b]	7.5 × 1.00	(M)	0.890	0.866	0.749 (0.657)
(GPE 102)		(T)	0.090	0.099	0.097 (0.105)
		(N)	0.020	0.035	0.154 (0.238)
I[c]	7.5 × 7.5	(M)	0.400	0.406	0.313 (0.273)
(GPE 102)		(T)	0.610	0.570	0.415 (0.340)
		(N)	−0.010	0.024	0.272 (0.387)
J[a]	7.5 × 7.8	(M)	0.478	0.502	0.400 (0.380)
(GPE 102)		(T)	0.474	0.489	0.400 (0.391)
		(N)	0.048	0.009	0.200 (0.229)

[a] Simultaneously two-way drawn
[b] Constant width
[c] Sequentially two-way drawn
[d] Values in brackets were calculated using Masuko's intrinsic birefringence values, whereas the others use Samuels' values

998 cm^{-1} peaks are also in good overall agreement, allowing for some sensitivity to less-ordered material.

1045 cm^{-1}. This peak is of similar width to the 998 cm^{-1} peak but of much lower intensity. The values of P_{200} are similar to but generally lower than those for the 841 cm^{-1} peak and show a rather larger scatter when plotted against them than those for the 998 cm^{-1} peak. The P_{220} values are similarly consistent with those for the 841 cm^{-1} peak, allowing for some sensitivity to less-ordered material.

973 cm^{-1}. The P_{200} values for this peak, shown in *Figure 6*, are significantly lower than those from the 841 cm^{-1} peak. These results are consistent with chains having the same alignment as those to which the 841 cm^{-1} peak is sensitive, provided that the absorption dipole for the 973 cm^{-1} peak makes an angle of about 23° with the chain axis. This angle is close to that found by Samuels[21] for this peak, viz. 18°. It was, however, necessary to fit this peak with two Lorentzians, one at 972 cm^{-1} of width 4.7 cm^{-1} and one at 974 cm^{-1} of width 7.3 cm^{-1}, and the results discussed so far were obtained by averaging over these two peaks.

Painter *et al.*[22] have shown by difference spectroscopy that the lower wavenumber peak corresponds to ordered material and the higher wavenumber peak to disordered material. If the data for the two peaks are processed separately this is confirmed. *Table 5* shows the $\langle \cos^2 \theta_{c,i} \rangle$ parameters obtained from the two separate peaks. *Figure 7* shows the P_{200} values for the two separate components and for the mean plotted against P_{200} for the 841 cm^{-1} peak and *Figure 8* shows a similar plot for the P_{220} values for the 972 cm^{-1} component plotted against the corresponding values for the 841 cm^{-1} peak. The behaviour of the 972 cm^{-1} peak is very similar to that of the 998 cm^{-1} peak. The 974 cm^{-1} peak shows a quite different behaviour. Its interpretation as an amorphous peak appears to be confirmed by comparing the $\langle \cos^2 \theta_M \rangle$ values calculated for this peak with those in *Table 4* deduced by combining the X-ray and optical data, as shown in *Figure 9*. Agreement with the values deduced using the limiting birefringences of Samuels is particularly good. When, however, the corresponding values of

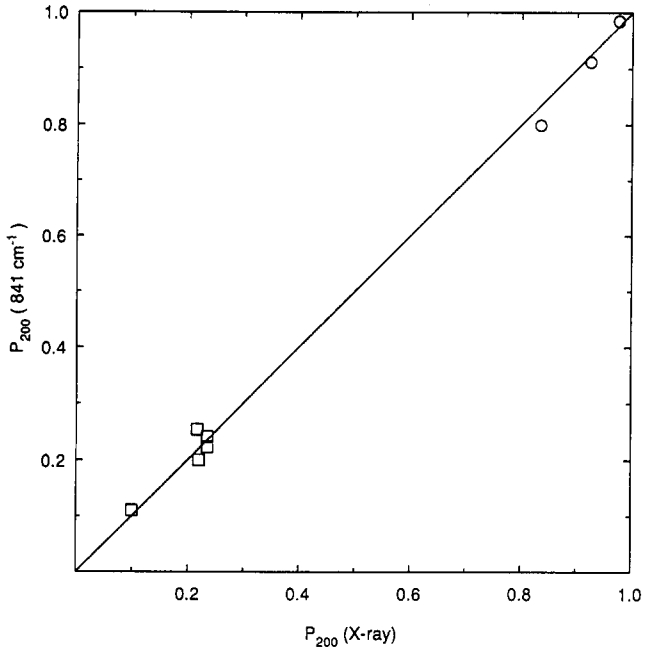

Figure 4 Comparison of P_{200} values obtained from X-ray diffraction and the 841 cm^{-1} infra-red peak: (□) two-way drawn samples (○) one-way drawn samples

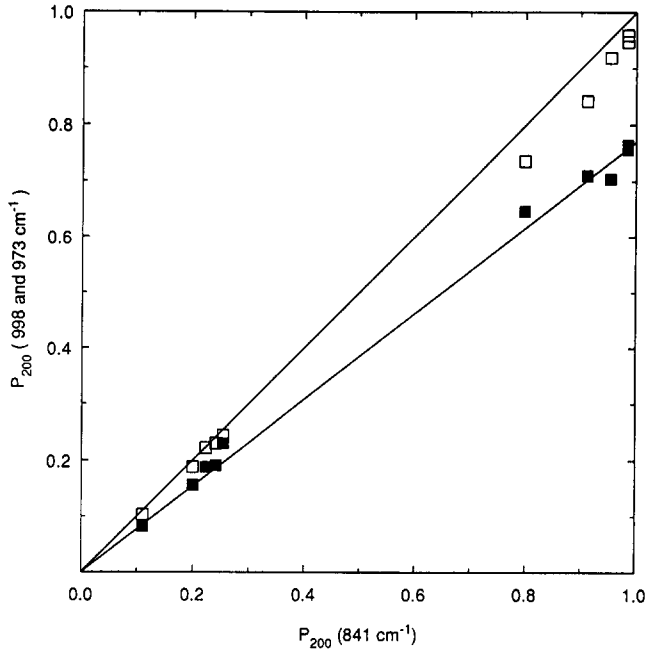

Figure 6 Comparison of P_{200} values obtained from the 841 cm^{-1} and the 998/973 cm^{-1} infra-red peaks: (■) 973 cm^{-1}; (□) 998 cm^{-1}

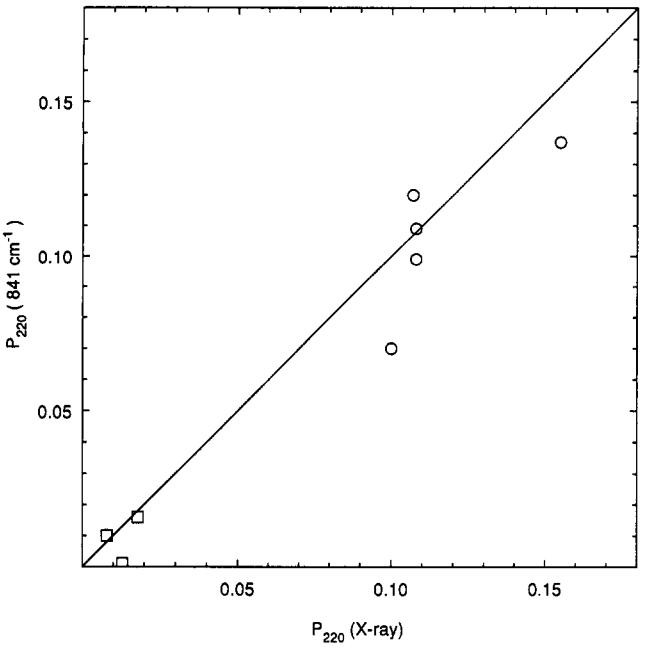

Figure 5 Comparison of P_{220} values obtained from X-ray diffraction and the 841 cm^{-1} infra-red peak. Notation for samples as in *Figure 4*

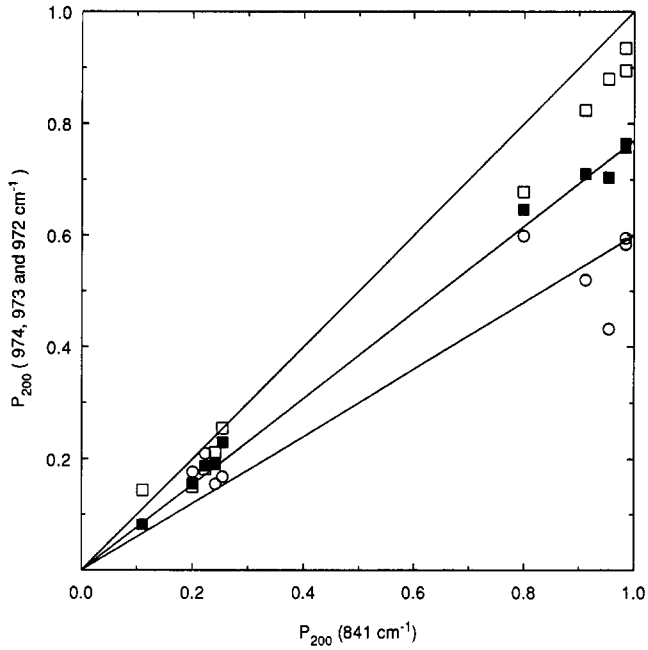

Figure 7 Comparison of P_{200} values obtained from the 841 cm^{-1} infra-red peak with those obtained from the 974 (○), 972 (□) and 973 cm^{-1} (■) infra-red peaks

$\langle \cos^2 \theta_T \rangle$ are compared the agreement is not as good and the reason for that is not understood. On average, the $\langle \cos^2 \theta_T \rangle$ and $\langle \cos^2 \theta_M \rangle$ values deduced from the 974 cm^{-1} peak suggest that the amorphous chains in the one-way drawn samples are approximately uniaxially oriented, with a slight tendency to be more oriented towards the plane of the film. The values deduced from the refractive index data using Samuels' limiting birefringences suggest a strong departure from uniaxiality in the opposite direction, which seems intuitively unlikely. It will therefore be assumed in any subsequent discussion that the 974 cm^{-1} peak gives somewhat more reliable information about the amorphous orientation than can at present be deduced from refractive index data.

Perpendicular modes

Values of P_{202} and P_{222} were deduced on the simplest hypothesis that the transition dipole for each of the perpendicular peaks is exactly perpendicular to the chain axis and that the values of P_{200} and P_{220} to be substituted in equations (12) and (13) are those from the 841 cm^{-1} peak, i.e. those for highly ordered material. The values of P_{202} and P_{222} obtained appear to differ systematically from zero, though only by a small amount of the same order as the experimental uncertainty. On the simplest assumption that no account need be taken of crystal field or correlation effects (no splittings are observed), it would be expected that the perpendicular modes, which

Table 5 Values of $\langle \cos^2 \theta \rangle$ for parallel polarization i.r. peaks

Sample	Draw ratio	Peak (cm^{-1})	$\langle \cos^2 \theta_{c,M} \rangle$	$\langle \cos^2 \theta_{c,T} \rangle$	$\langle \cos^2 \theta_{c,N} \rangle$
A	8.5 × 0.90	973	0.807	0.120	0.073
(ICI PP)		972	0.883	0.101	0.016
		974	0.680	0.152	0.168
B	9.5 × 0.96	973	0.803	0.108	0.089
(ICI PP)		972	0.920	0.062	0.018
		974	0.621	0.180	0.199
C	12.0 × 0.75	973	0.838	0.066	0.096
(ICI PP)		972	0.930	0.056	0.014
		974	0.730	0.144	0.126
D	14.0 × 0.77	973	0.843 ∓ 0.003	0.104 ∓ 0.003	0.053 ∓ 0.002
(ICI PP)		972	0.956	0.036	0.008
		974	0.722	0.176	0.102
H	7.5 × 1.0	973	0.764	0.164	0.072
(GPE 102)		972	0.785	0.153	0.062
		974	0.732	0.183	0.085
E[a]	4.5 × 4.5	973	0.437	0.394	0.169
(ICI PP)		972	0.433	0.393	0.174
		974	0.452	0.398	0.150
F[a]	6.0 × 6.1	973	0.461 ∓ 0.002	0.432 ∓ 0.004	0.107 ∓ 0.004
(ICI PP)		972	0.475	0.441	0.084
		974	0.437	0.415	0.148
G[a]	7.5 × 7.5	973	0.459	0.454	0.087
(ICI PP)		972	0.455	0.452	0.093
		974	0.473	0.459	0.068
I[b]	7.5 × 7.5	973	0.388	0.511	0.101
(GPE 102)		972	0.429	0.545	0.026
		974	0.306	0.444	0.250
J[a]	7.5 × 7.8	973	0.487	0.479	0.034
(GPE 102)		972	0.503	0.493	0.004
		974	0.445	0.444	0.111

[a] Simultaneously two-way drawn
[b] Sequentially two-way drawn

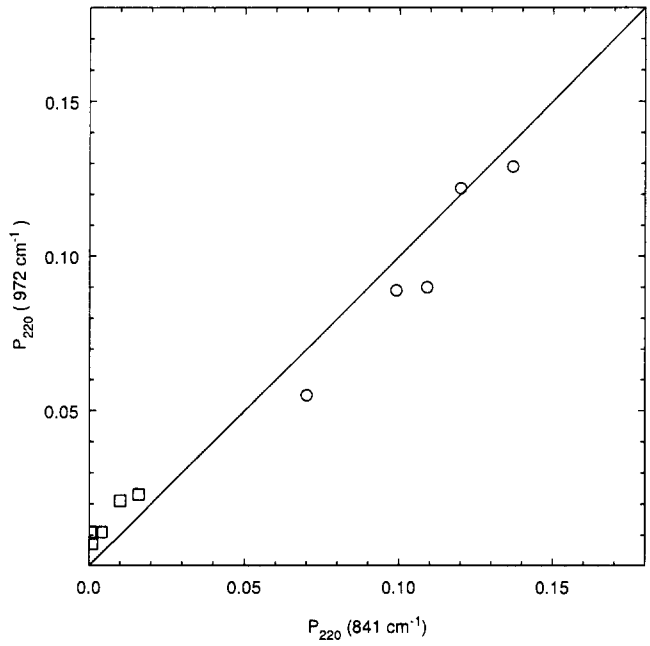

Figure 8 Comparison of P_{220} values obtained from the 972 cm^{-1} and 841 cm^{-1} infra-red peaks. Notation for samples as in *Figure 4*

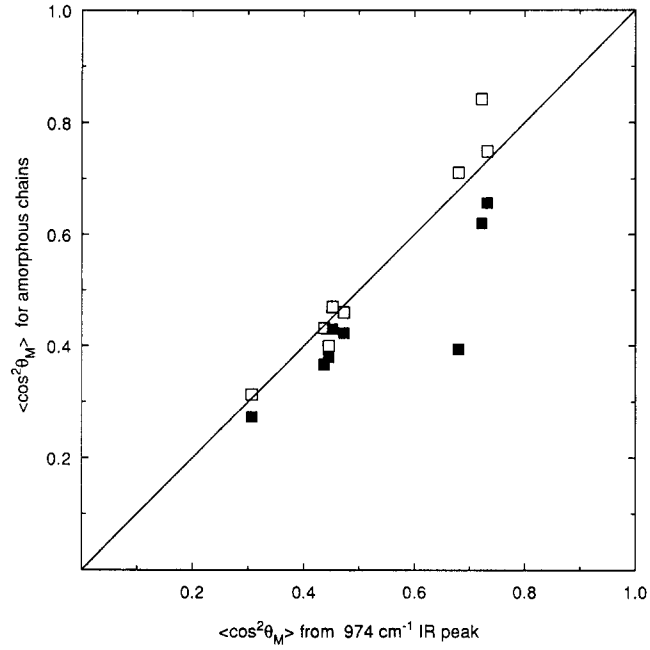

Figure 9 Comparison of $\langle \cos^2 \theta_M \rangle$ values obtained from the 974 cm^{-1} infra-red peak with those obtained for amorphous chains by combining X-ray diffraction and refractive index data using intrinsic birefringence values from Samuels (□) and Masuko (■)

are doubly degenerate E modes, would show zero values for these quantities. Possible explanations for the observed results are still under consideration.

Description of the state of orientation of the samples

Figure 10 shows $\langle\cos^2\theta_{c,M}\rangle$ plotted against $\langle\cos^2\theta_{c,T}\rangle$ using the X-ray data from *Table 2*, and *Figure 11* shows a similar plot using the i.r. data for the 841 cm^{-1} peak. Both plots show that the points for the one-way drawn samples cluster in a region of high orientation somewhere between uniaxial orientation with respect to the draw direction and in-plane orientation, as expected. Despite the high orientation observed at a draw ratio of 8.5 x 0.90, further orientation takes place up to the highest draw ratio studied, 14.0 x 0.77.

The simultaneously two-way drawn samples cluster near the in-plane equibiaxial point, again as expected. The X-ray data show very little difference in orientation for all these samples, but the i.r. data suggest a slight increase in the degree of planar orientation with increasing draw ratio for samples E, F and G (ICI PP) and suggest that sample J (GPE 102) is more oriented than sample G, although they were drawn to essentially the same draw ratio. These differences may reflect the fact that the i.r. results are sensitive to some non-crystalline chains which may be slightly less oriented than the crystalline chains. Both plots show that the sequentially two-way drawn sample, I (GPE 102), although drawn to essentially the same final draw ratios as samples J and G, has a high degree of planar orientation of the chain axes but does not lie near the equibiaxial line; the chains are significantly more oriented towards the final draw direction than towards the initial draw direction.

Figure 12 shows a similar plot to *Figures 9* and *10*, but using data from the 974 cm^{-1} i.r. peak which, as discussed above, reflects the orientation of the non-crystalline chains. All three types of sample show

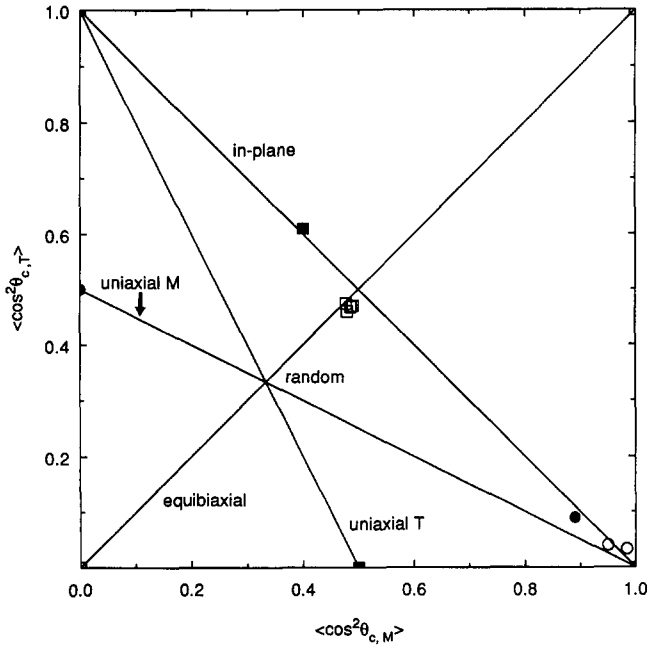

Figure 10 Comparison of $\langle\cos^2\theta_{c,M}\rangle$ and $\langle\cos^2\theta_{c,T}\rangle$ using X-ray diffraction data: (○) one-way drawn samples A and D; (●) one-way drawn sample H; (□) simultaneously two-way drawn samples E, F, G and J; (■) sequentially two-way drawn sample I

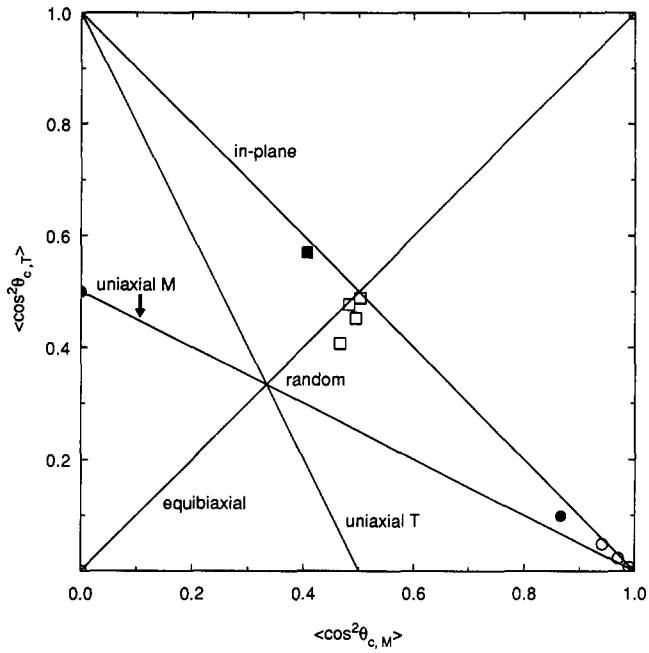

Figure 11 Comparison of $\langle\cos^2\theta_{c,M}\rangle$ and $\langle\cos^2\theta_{c,T}\rangle$ using the 841 cm^{-1} infra-red peak parameters: (○) one-way drawn samples A, B, C and D; (●) one-way drawn sample H; (□) simultaneously two-way drawn samples E, F, G and J; (■) sequentially two-way drawn sample I

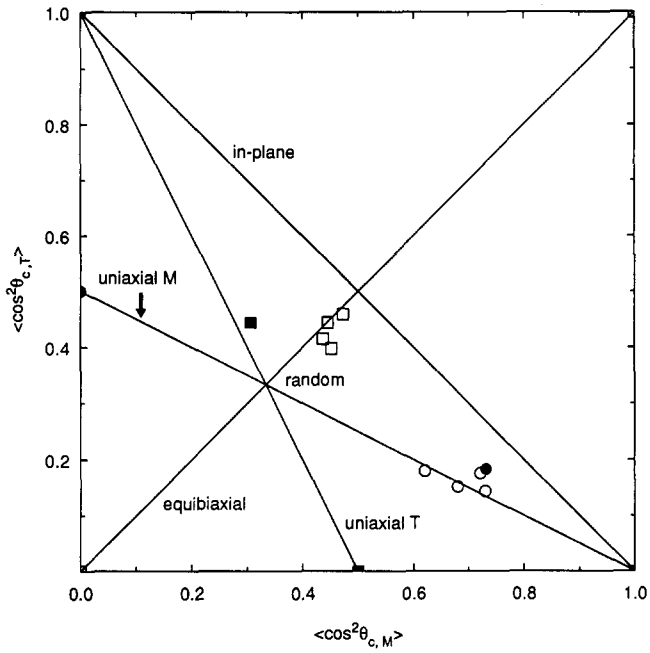

Figure 12 Comparison of $\langle\cos^2\theta_{c,M}\rangle$ amd $\langle\cos^2\theta_{c,T}\rangle$ using the 974 cm^{-1} infra-red peak parameters. Notation for samples as in *Figure 11*

a significantly lower degree of orientation for the amorphous chains than for the crystalline chains. The simultaneously two-way drawn samples still cluster near the equibiaxial line, as expected. The one-way drawn samples tend to lie very close to the line corresponding to uniaxial orientation with respect to the draw direction and the point for the sequentially two-way drawn sample lies very close to the line corresponding to uniaxial orientation with respect to the second draw direction.

The X-ray data can provide information about the orientations of the a and b crystallographic axes as well as that of the c-axis. The data in *Table 2* show that for

all the samples the b-axis is preferentially oriented normal to the plane of the sample and that it becomes increasingly so oriented as the simultaneous two-way draw ratio increases. For the sequentially two-way drawn sample the b-axis appears to be slightly more oriented towards the normal to the sheet than it is for the simultaneously two-way drawn sample of the same material and the same final draw ratios.

It is not possible to deduce from the data presented here anything about the mechanism of the change of orientation of the c-axes in the sequentially two-way drawn sample from being approximately parallel to the original draw direction to being more parallel to the final draw direction. X-ray studies on similar samples have, however, shown that the orientation changes smoothly from one orientation to the other and there is no evidence of two populations of crystallites. The mechanism thus appears to be predominantly one of rotation of crystallites rather than one of breakdown and recrystallization, although the crystallinity falls slightly during the second draw.

CONCLUSIONS

It has been shown that X-ray diffraction, infra-red spectroscopy and refractive index measurements taken together can provide a much firmer basis for characterizing the molecular orientation distribution in polypropylene than can be provided by measurements using only two of the techniques. The results show that the 841 cm^{-1} i.r. peak gives information about the chain axes which is very similar to that given by the X-ray data for crystallites, but it is possible that this peak has some slight sensitivity to ordered lengths of chain not contained in crystallites. The 973 cm^{-1} peak contains two components, one of which can give information directly about non-crystalline chains. The close agreement of the orientation parameters deduced from this peak with those deduced indirectly from refractive index data gives confidence in the values of the parameters. Best agreement is obtained when the maximum birefringences of Samuels are used in analysing the refractive index data. The 841 and 973 cm^{-1} peaks thus form an alternative pair of peaks for the determination of crystalline and amorphous orientation to the peaks at 1220 and 2725 cm^{-1} used by Mirabella[5].

Polypropylene becomes quite highly oriented at relatively low draw ratios, whether drawn one-way or two-way, but the amorphous material remains significantly less oriented than the crystalline material even at the highest draw ratios studied here. This result is consistent with Mirabella's work for uniaxially oriented polypropylene[5]. The most interesting result is that for the sequentially two-way drawn sample. Although it was drawn to the same draw ratio in the two directions the chains became significantly more oriented towards the second draw direction than towards the first. The crystalline chains were oriented close to the plane of the sample but the amorphous chains were almost uniaxially oriented with respect to the second draw direction. Further studies on sequentially drawn samples produced under more closely defined drawing conditions would be desirable, and measurements by Raman spectroscopy might be able to provide more information on the nature of the orientation distribution function for the non-crystalline chains.

REFERENCES

1 Unwin, A. P., Bower, D. I. and Ward, I. M. *Polymer* 1985, **26**, 1605
2 Taraiya, A. K., Unwin, A. P. and Ward, I. M. *J. Polym. Sci., Polym. Phys. Edn* 1988, **26**, 817
3 Samuels, R. J. *J. Appl. Polym. Sci.* 1981, **26**, 1383
4 Kissin, Y. V. *J. Polym. Sci.* 1983, **21**, 2085
5 Mirabella, F. M. *J. Polym. Sci., Polym. Phys. Edn* 1987, **25**, 591
6 Taraiya, A. K., Orchard, G. A. J. and Ward, I. M. *J. Appl. Polym. Sci.* 1990, **41**, 1659
7 Unwin, A. P. *PhD Thesis* University of Leeds, 1983
8 Taraiya, A. P. *PhD Thesis* University of Leeds, 1988
9 Jarvis, D. A., Hutchinson, I. J., Bower, D. I. and Ward, I. M. *Polymer* 1980, **21**, 41
10 Roe, R. J. *J. Appl. Phys.* 1965, **36**, 2024
11 Taraiya, A. K., Orchard, G. A. J. and Ward, I. M. *Plast. Rubber Comp. Proc. Appl.* in press
12 Natta, G. *J. Polym. Sci.* 1955, **16**, 143
13 Wilchinsky, Z. W. *Adv. X-ray Anal.* 1962, **6**, 231
14 Alexander, L. E. 'X-ray Diffraction Methods in Polymer Science', Wiley, New York, 1969, p. 198
15 Geiss, D. and Hoffman, D. *Prog. Polym. Sci.* 1990, **15**, 1
16 Decker, B. F., Asp, E. T. and Harker, D. *J. Appl. Phys.* 1948, **19**, 388
17 Green, D. I. and Bower, D. I. *Spectrochim. Acta* in press
18 Spiby, P. *PhD Thesis* University of Leeds, 1988
19 Masuko, T., Tanaka, H. and Okajima, S. *J. Polym. Sci. (A-2)* 1970, **8**, 1565
20 Kissin, Yu. V. and Rishina, L. A. *Eur. Polym. J.* 1976, **12**, 757
21 Samuels, R. J. *Makromol. Chem., Suppl.* 1981, **4**, 241
22 Painter, P. C., Watzek, M. and Koenig, J. L. *Polymer* 1977, **18**, 1169